Effects of anisotropy on the development of cardiac arrhythmias associated with focal activity

Wilders, R.; Wagner, M.B.; Golod, D.A.; Kumar, R.; Wang, Y.G.; Goolsby, W.N.; Joyner, R.W.; Jongsma, H.

DOI
10.1007/s004240000413

Publication date
2000

Published in
Plügers Archiv

Pflügers Arch - Eur J Physiol (2000) 441:301–312
DOI 10.1007/s004240000413

ORIGINAL ARTICLE

**Ronald Wilders · Mary B. Wagner · David A. Golod
Rajiv Kumar · Yang-Gan Wang · William N. Goolsby
Ronald W. Joyner · Habo J. Jongsma**

Effects of anisotropy on the development of cardiac arrhythmias associated with focal activity

Received: 23 May 2000 / Received after revision: 13 July 2000 / Accepted: 14 July 2000 / Published online: 1 September 2000

Abstract The anisotropy that normally exists in the myocardium may be either enhanced in peri-infarction zones by loss of lateral cell connections or reduced by redistribution of gap junctions. To test how the degree of anisotropy affects the development of ectopic focal activity, we carried out computer simulations in which a model of an ectopic focus is incorporated as the central element of a two-dimensional sheet of ventricular cells. At low values of intercellular coupling conductance (G_c), the focus region is spontaneously active, but the limited intercellular current flow inhibits propagation. At high G_c, automaticity is suppressed by the loading effects of the surrounding cells. At intermediate G_c, the ectopic activity may propagate into the sheet. In the case of isotropic coupling, the minimum size of the focus region for propagation to occur (in terms of number of collaborating cells within the focus) is as small as approximately ten cells, and this number decreases with increasing anisotropy. Thus, the presence of anisotropy facilitates the development of ectopic focal activity. We conclude that the remodeling that occurs in peri-infarction zones may create a substrate that either *facilitates* (enhanced anisotropy) or *inhibits* (reduced anisotropy) the development of cardiac arrhythmias associated with ectopic focal activity.

R. Wilders (✉) · H.J. Jongsma
University Medical Center Utrecht,
Department of Medical Physiology,
PO Box 85060, 3508 AB Utrecht, The Netherlands
e-mail: r.wilders@med.uu.nl
Tel.: +31-30-2538900, Fax: +31-30-2539036

R. Wilders
Academic Medical Center, University of Amsterdam,
Department of Physiology, Amsterdam, The Netherlands

M.B. Wagner · D.A. Golod · R. Kumar · Y.-G. Wang
W.N. Goolsby · R.W. Joyner
Todd Franklin Cardiac Research Laboratory,
The Children's Heart Center, Department of Pediatrics,
Emory University, Atlanta, GA, USA

Keywords Anisotropy · Computer simulations · Electrophysiology · Gap junctions · Heart · Ischemia · Ventricular cells

Introduction

Many experimental and theoretical studies have focused on action potential propagation in cell pairs, linear strands, or multi-dimensional structures of cardiac cells. Multi-dimensional cardiac tissue differs in conduction behavior from the simple linear models in several respects. Myocyte structure is asymmetrical, with average adult myocytes being 100–150 μm in length and 15–25 μm in width [13, 23], with the cellular arrangement of these cells giving the tissue a structural anisotropy. Anisotropy is further enhanced by the spatial distribution of gap junctions – ensembles of intercellular ion channels providing the electrical pathway between neighboring cells– such that the propagation velocity in the transverse direction is lower than that in the longitudinal direction, with ratios of 1 to 2.7 in the ventricle and up to 1 to 12 in the atrial crista terminalis [2, 11, 19, 36].

The interactions among heart cells with spatial variability in action potential properties and intercellular coupling are even more complex in the ischemic heart. Cellular electrophysiological dysfunction may lead to conduction slowing and/or block which may facilitate reentrant arrhythmias, or, alternatively, to localized areas of ectopic activity which may generate non-reentrant arrhythmias. Numerous studies of healed infarctions in ventricular tissue have shown fractionated electrical activity indicative of the partial electrical uncoupling of groups of cells [10, 18, 37]. Direct evidence for reduced coupling between cells comes from immunohistochemical studies showing that there are smaller and fewer gap junctions in peri-infarction zones [24, 32]. Anisotropy may be enhanced by a particular loss of lateral connections compared to end-to-end connections among heart cells [24]. On the other hand, anisotropy may be reduced by a redistribution of gap junctions, tending to become

randomly spread over the cell surfaces, and not in discrete intercalated disks at the end-to-end cell contacts as in normal myocardium [24, 32]. Many episodes of acute ischemia occur in such "abnormal" tissue, i.e., that has a spatially inhomogeneous distribution of intercellular coupling resulting from prior injury, which may serve as a substrate from which arrhythmias can arise [26].

The actual membrane properties of cells of a pathologically present ectopic focus are not clearly known. Recent microelectrode recordings from an ectopic focus area removed from a patient with atrial tachycardia [3] showed a group of depolarized, spontaneously active cells which, under the in vitro conditions of the recordings, showed considerable electrical uncoupling from the surrounding atrial cells. Several types of heart cells within the normal heart express spontaneous diastolic depolarization which can lead to focal activity either as a normal process (e.g., the sinoatrial node) or as an abnormal process (e.g., the atrio-ventricular node, the coronary sinus region, or the Purkinje system). In our previous work, in which we studied the electrical interactions between a spontaneously pacing cell model representing an ectopic focus and a real, isolated ventricular myocyte [20, 38], we used our previously published sinoatrial cell model [40] as a model of the ectopic focus. Even at this level of a pair of cells with different membrane properties, the anatomical properties that organize cardiac cells into functional groups could be seen to play a critical role in enabling propagation.

The multiple effects of anisotropy on an already propagating wave, produced by direct stimulation, have been widely studied, both in computer simulations [7, 15, 21, 34] and in cell culture systems with cultures grown on a directed collagen matrix to form an anisotropic network [5, 6]. We recently extended our "coupling clamp" technique in which we couple a real cell to a real-time simulation of a model cell to incorporate a real cardiac cell as the central element of a two-dimensional sheet of model cells [39]. In this sheet composed of 7×7 elements the coupling conductances may be different in the *X* and *Y* directions and a specific region of lack of coupling conductance may serve as a resistive barrier. We determined the critical size for the successful propagation from a directly stimulated real ventricular cell in the central location into the sheet, and found that this critical size was decreased when anisotropy was present compared to when it was not, and was further decreased when the central site of stimulation was close to a resistive barrier.

Much less work has been done on the effects of anisotropy on the *initiation* of a propagating wave of excitation. The critical size of an automatic focus region was the subject of our previously published theoretical study [16], in which we simulated a two-dimensional sheet of atrial tissue with a centrally located sinoatrial node area of variable size. In this study, we showed that a partial electrical uncoupling between the automatic area and the quiescent area was required in order for the automatic area to maintain automaticity and still drive the quiescent area. Generation and propagation of the sinoatrial nodal impulse in a two-dimensional sheet of cells has also been studied in large-scale simulations on a massively parallel computer [1]. Winslow et al. [43] used similar simulation techniques to study the generation of ectopic activity in an isotropic two-dimensional sheet of atrial cells, into which a region of inhibited sodium–potassium pump activity was incorporated. They demonstrated that the local sodium overloading produced by the pump inhibition can induce propagating ectopic beats, with the critical size of the overload region for generating propagating ectopic beats depending on the cell-to-cell coupling magnitude.

The initiation of a propagating wave from an automatically active focus involves the input resistance of the syncytial tissue, the ability of the focus region to serve as a current source, and the sensitivity of the focus region to electrotonic interactions with the surrounding quiescent region which will tend to either abolish automaticity or prevent the initiation of propagation. In order to study the way in which anisotropic connectivity affects the initiation of a propagating wave, we carried out computer simulations using a two-dimensional sheet of ventricular cells into which a spontaneously active cell model is incorporated as a central focus element, and for which the intercellular conductances in the *X* and *Y* directions can be varied to introduce anisotropy.

Materials and methods

Two-dimensional sheet

The diagram of Fig. 1 illustrates the two-dimensional sheet we simulated composed of 13×13=169 elements. Each element (except those on the edges of the sheet) has resistive coupling to four adjacent elements and the (ohmic) coupling conductances are assumed to be a constant G_x along the *X*-axis and a possibly different constant G_y along the *Y*-axis. Elements for the central portion of the sheet are numbered along the *X*- and *Y*-axes as –2, –1, 0, 1, and 2. The numbering of the entire sheet extends from –6 to +6 along each axis as indicated. The upper right quadrant (thick lines) consists of 49 elements for which the focus cell at (0,0) (filled square in the center of the total sheet) is at the lower left position. We achieve horizontal and vertical symmetry by the condition that only the central element at (0,0) or the 9 elements in the central 3×3 array (black and gray squares) are spontaneously active. From symmetry, we can then include all of the interactions among elements in the entire sheet by solving only for the potential and coupling currents of the 49 elements of the upper right quadrant, even if G_x and G_y are not equal to each other.

To represent all of these interactions, we let $I_x(i,j)=G_x\cdot(V_{i,j}-V_{i+1,j})$ be the (ohmic) current which flows to the right of element (i,j), where $V_{i,j}$ is the membrane potential of element (i,j). For the elements on the left edge of the upper right quadrant [elements (0,0), (0,1), … (0,6)] we double the computed I_x to include the current which, from symmetry, would have flowed in the opposite direction along the *X*-axis. Similarly, we let $I_y(i,j)=G_y\cdot(V_{i,j}-V_{i,j+1})$ be the current which flows up along the *Y*-axis and we double this current for the elements along the bottom edge of our upper right quadrant [elements (0,0), (1,0), (2,0), … (6,0)] to include the current which would have flowed in the opposite direction down the *Y*-axis for these elements. Thus, the central element (which has intrinsic spontaneous activity) gets both its I_x and I_y doubled, since it is on both edges. For the other elements in the upper right quadrant the definitions for I_x and I_y are as given except for the edge elements where the coupling current either to the right or up is zero [I_x=0 for elements (6,0), (6,1), … (6,6) and I_y=0 for elements (0,6), (1,6), … (6,6)]. We thus reduce the problem of solving a sheet of 169 elements to a problem of solving for only 49 elements.

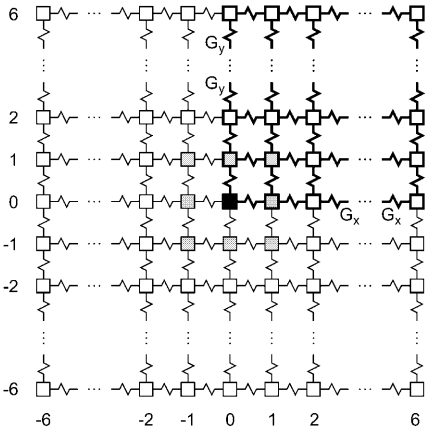

Fig. 1 Diagram of a two-dimensional sheet of ventricular cells composed of 13×13 elements with a central area of focal activity. Each coupling conductance in the *X* direction has value G_x (nS) and each coupling conductance in the *Y* direction has value G_y (nS). The central focus element at (0,0) is represented by the nodal cell model of Wilders et al. [40] with its membrane capacitance and currents scaled by a factor of 5 to account for the difference in size between nodal and ventricular cells (focus model, *central black square*). The other elements are represented by the phase-2 ventricular cell model of Luo and Rudy [25] as updated by Zeng et al. [44] (LR model, *open squares*). Elements directly surrounding the central element (*gray squares*) are represented by either the focus model or by the LR model. The upper right quadrant of 49 elements (*thick lines*) is actually solved (see "Materials and methods")

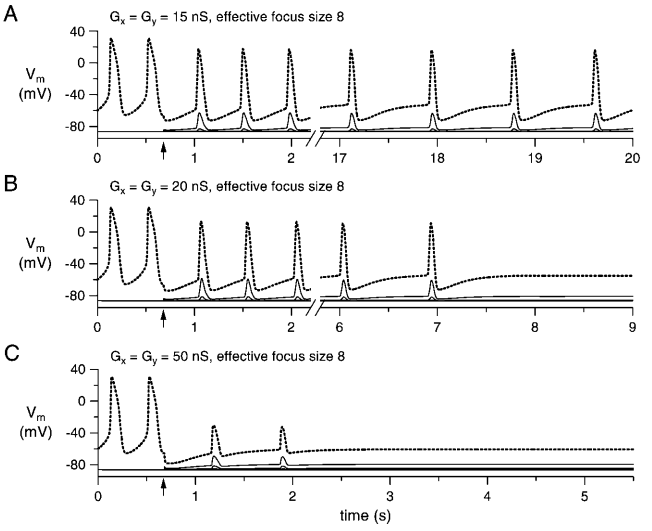

Fig. 2A–C Action potential propagation from the central focus element at (0,0) with a size factor of 8 into the two-dimensional sheet of Fig. 1 with G_x=G_y (isotropic sheet). Each *panel* shows the membrane potential (V_m) for elements 0, 1, …, 6 along the middle row of elements (*Y*=0), with the activity of the focus element (element 0) shown as a *dotted line*. Coupling is turned on at the time indicated by the *vertical arrows*. Note axis breaks. **A** Failure of propagation ("pace but not drive") at G_x=G_y=15 nS. **B** Failure of propagation ("not pace") at G_x=G_y=20 nS. **C** Failure of propagation ("not pace") at G_x=G_y=50 nS

Membrane models and numerical integration

The membrane model we use for the spontaneously active element at the center of the sheet is our previously published sinoatrial node model [40] (SAN model), with its 32-pF membrane capacitance and its currents scaled by a factor of 5 to account for differences in size between the SAN model cell and real ventricular cells. Thus, the "size 1" focus element has a membrane capacitance of 160 pF, similar to the value of 153.4 pF for the remaining elements in the sheet, which are represented by the phase-2 ventricular cell model of Luo and Rudy [25], as modified by Zeng et al. [44] (LR model).

In this study we use a simple first-order numerical integration scheme with a fixed time step of 5 μs. At each time step, the (ohmic) coupling currents are calculated as described above and then are used together with the calculated membrane currents for each element to integrate the membrane potential for each element of the array. In this implementation of a two-dimensional array of cells, we have treated each element of the array (except the central element) as one isopotential cell. We allow the effective size of this central element to be varied, as if this element represents a small cluster of *N* cells infinitely well coupled to each other. The effective size of this central element can be varied by simply scaling the coupling currents associated with that element. To increase the effective size of this element by a factor of *N*, so that it represents *N* focus cells, its membrane potential is integrated with its computed coupling currents divided by *N*, as we have previously described in detail [41, 42].

We followed a protocol in which we first ran the simulation with the central element uncoupled from the sheet for two cycles of automaticity and then coupled the central element and the other elements of the sheet with desired values of G_x and G_y for at least 20 s to allow development of steady-state behavior (see Figs. 2, 3). The simulations were coded and compiled using Active Ada (version 5.3, Alsys, Boston, Mass., USA) and run on a personal computer equipped with a 450-MHz Pentium II processor. Typical computation time for a 20-s simulation was ≅20 min.

Results

Activation of an isotropic sheet

Figure 2 illustrates the effects of coupling a central focus element into the 13×13 element sheet as diagrammed in Fig. 1. Each element, except the central one, is represented by the LR model and the central element is represented by the focus model with the size set to 8 (see Materials and methods). This size setting makes the central element equivalent to 8 focus cells with infinitely good coupling among these 8 cells such that they can act as a unit to provide current to the surrounding elements of the sheet. For this example we set G_x=G_y so that the sheet is isotropic. The results are plotted in three panels for G_x=G_y values of 15, 20, and 50 nS, respectively. Each panel shows results for elements 0, 1, …, 6 along the middle row of the sheet. The data displayed are the last two action potentials that occurred in the central element while it was uncoupled from the rest of the sheet, followed by the activity which develops over the ≅19-s period after coupling was established.

In Fig. 2A (G_x=G_y=15 nS), the focus element (0,0) shows two action potentials during the uncoupled period and then, after coupling has been turned on (vertical arrow), a train of action potentials which do not propagate into the sheet (thick dotted line). In the ventricular cells (1,0), (2,0), … (6,0) (thin solid lines), only subthreshold depolarizations are observed, which are largest in adjacent cell (1,0). At this value of coupling conductance, the focus element continues to pace upon coupling (at a

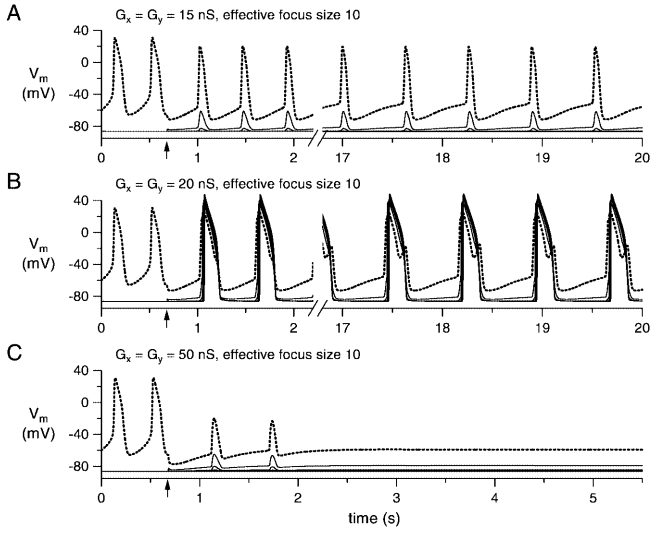

Fig. 3A–C Action potential propagation from the central focus element at (0,0) with a size factor of 10 into the two-dimensional sheet of Fig. 1 with G_x=G_y (isotropic sheet). Each *panel* shows the membrane potential (V_m) for elements 0, 1, …, 6 along the middle row of elements (Y=0), with the activity of the focus cell (element 0) shown as a *dotted line*. Coupling is turned on at the time indicated by the *vertical arrows*. Note axis breaks. **A** Failure of propagation ("pace but not drive") at G_x=G_y=15 nS. **B** Successful propagation ("pace and drive") at G_x=G_y=20 nS. **C** Failure of propagation ("not pace") at G_x=G_y=50 nS

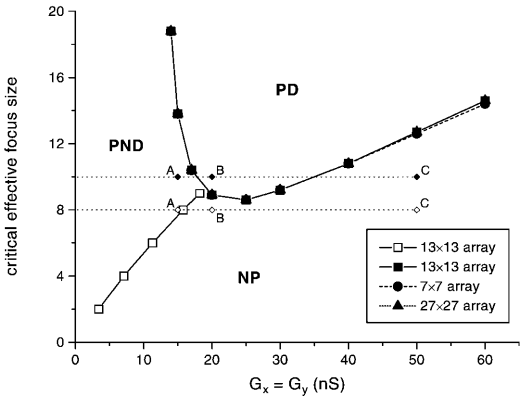

Fig. 4 Critical size factor for successful propagation from the central focus element into the 13×13 element sheet as diagrammed in Fig. 1 with G_x=G_y (*solid line with filled squares*). Results for smaller and larger sheets are shown as a *dashed line with filled circles* (7×7 element sheet) and a *dotted line with filled triangles* (27×27 element sheet), respectively. Successful propagation occurs for parameter values in the region labeled "*PD*" ("pace and drive"). Failure of propagation occurs either as a failure to drive ("pace but not drive", region labeled "*PND*") or as a failure to pace ("not pace", region labeled "*NP*"). The *solid line with open squares* marks the transition between the PND and NP regions. The *horizontal dashed line with open diamonds* at focus size 8 marks the parameter values used for *panels* **A**, **B**, and **C** of Fig. 2 as indicated. Similarly, the *horizontal dashed line with filled diamonds* at focus size 10 marks the parameter values used in Fig. 3

slower rate as compared to the uncoupled state due to the loading effects of the sheet), but it does not drive the sheet ("pace but not drive"). The low coupling conductance inhibits current flow into the other sheet elements and thus activation of the sheet does not occur.

If we now increase coupling conductance to 20 nS, and thus increase coupling current, we observe the results shown in Fig. 2B. The increased coupling current induces larger depolarizations in the adjacent cells, but these are still subthreshold. After a ≅6-s period of increasing interbeat intervals spontaneous activity of the focus element ceases due to increased loading effects as compared to the previous case of G_x=G_y=15 nS. A further increase in coupling conductance to 50 nS (Fig. 2C) leads to almost instantaneous cessation of automaticity. After coupling is established there are only two action potentials in the focus element which are very depressed in amplitude due to the increased electrotonic loading of the sheet and thus activation of the sheet does not occur. At these higher values of coupling conductance (20 and 50 nS), automaticity is suppressed by the loading effects of the surrounding cells ("not pace"). At an effective focus size of 8, there was no value of coupling conductance which allowed sustained successful propagation into the sheet.

If we now increase the effective size of the focus to 10, and thus reduce the loading effects of the sheet, we obtain the results shown in Fig. 3 (same format as Figure 2) for the same G_x=G_y values of 15, 20, and 50 nS. At a coupling conductance of 15 nS (Fig. 3A), we again observe "pace but not drive" activity (see Fig. 2A). The depolarizations in the ventricular cells (thin solid lines) are still subthreshold, but these depolarizations now have a larger amplitude due to the reduced loading effects. Also, the decrease in pacing rate is less pronounced. The low coupling conductance inhibits current flow into the other sheet elements and thus activation of the sheet does not occur. If we increase coupling conductance to 20 nS (Fig. 3B), the depolarizations in the adjacent ventricular cells reach threshold and sustained successful propagation into the sheet develops ("pace and drive"). However, a further increase in coupling conductance to 50 nS (Fig. 3C) leads to almost instantaneous cessation of automaticity as previously shown in Fig. 2C for a focus size factor of 8. At an effective focus size of 10, there is a "window" of intermediate values of coupling conductance which allow sustained successful propagation into the sheet.

Critical size factor

When we ran a large number of these simulations, always keeping G_x=G_y, we were able to delineate the relationship between the value of G_x (=G_y) and a critical size factor for the central focus element (the size factor below which the sheet was not activated and above which the sheet was activated), as shown in Fig. 4 as the solid line and filled square symbols. This relationship thus defines a region of parameter values for which successful action potential propagation into the sheet is observed ("pace and drive", region labeled "PD"). The three examples shown in Fig. 2 were all run with a size factor of 8, as indicated by the dashed horizontal line and the open diamonds along this

line marked “A” (for Fig. 2A), “B” (for Fig. 2B), or “C” (for Fig. 2C). Similarly, the examples shown in Fig. 3 are indicated by the closed diamonds along the dashed horizontal line at effective focus size 10. Note that the relationship for the critical effective size for successful driving of the sheet has a minimum value of a size factor of 8.6 for the central element and this minimum value occurs at G_x=G_y=25 nS. Thus, for these particular cell membrane models, there is no set of G_x (=G_y) values which would enable activation of the sheet for a central element size factor less than 8.6. For larger size factors of the central element, the set of values of G_x (=G_y) for which activation of the sheet can occur is limited to values greater than about 13 nS, and, with values of G_x (=G_y) greater than 25 nS, is limited by a progressively increasing critical size factor.

Effects of sheet size

To test whether the size of our two-dimensional sheet, i.e., the 13×13 element sheet as diagrammed in Fig. 1, is sufficient to simulate the electrotonic loading effects of a sheet of ventricular cells on a central focus element, we repeated our simulations with larger and smaller arrays. The smaller sheet we used had 7×7 elements and thus each row (and column) had elements –3 through 3 instead of –6 through 6 (see Fig. 1). The larger sheet was composed of 27×27 elements with elements –13 through 13 along each row (and column). The results obtained with the larger sheet are plotted in Fig. 4 as a dotted line with closed triangles. At all values of coupling conductance tested the results were identical to those obtained with the “standard” 13×13 element sheet, indicating that the 13×13 sheet is sufficiently large. Actually, the results for the smaller sheet, plotted in Fig. 4 as a dashed line with closed circles, were very close to those obtained with the 13×13 and 27×27 arrays. Only at coupling conductances >40 nS, resulting in larger space constants, was the critical size factor slightly underestimated.

Two types of propagation failure

The other relationship shown in Fig. 4 with a solid line and open squares is the relationship obtained when we ran simulations to determine the type of action potential propagation failure in the “not-PD” region. This relationship marks the transition between two regions of parameter values with different types of propagation failure, labeled “PND” and “NP”. At low values of coupling conductance, only little coupling current flows into the sheet. As a consequence, the central focus element paces but it is not able to drive the sheet. Failure of action potential propagation thus occurs as “pace but not drive” (PND) as illustrated in Figs. 2A and 3A. At higher values of coupling conductance, the spontaneous activity of the central focus element is suppressed due to increased electrotonic loading effects and propagation failure then occurs as “not pace” (NP) as illustrated in Figs. 2B,C and 3C.

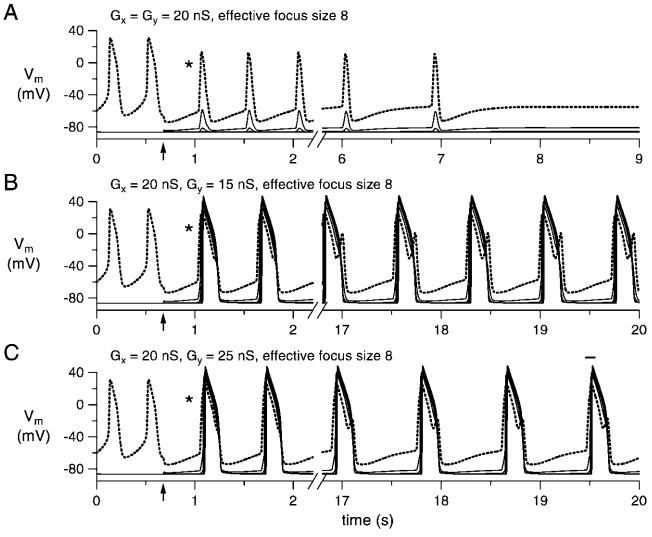

Fig. 5A–C Effects of anisotropy on action potential propagation from the central focus element at (0,0) with a size factor of 8 into the two-dimensional sheet of Fig. 1. Each *panel* shows the membrane potential (V_m) for elements 0, 1, …, 6 along the middle row of elements (Y=0), with the activity of the focus cell (element 0) shown as a *dotted line*. Coupling is turned on at the time indicated by the *vertical arrows*. *Asterisks* indicate the action potentials of the central focus element for which the associated coupling currents are shown in Fig. 6. Note axis breaks. **A** Failure of propagation in the isotropic case of G_x=G_y=20 nS. **B** Successful propagation upon introduction of anisotropy by *decreasing* G_y to 15 nS. **C** Successful propagation upon introduction of anisotropy by *increasing* G_y to 25 nS. The *horizontal bar* near time 19.5 s indicates the 80-ms period shown at a faster time scale in Fig. 7

Activation of an anisotropic sheet

We now consider the effects of making an isotropic sheet into an anisotropic sheet by either decreasing or increasing the value of G_y while maintaining a constant value of G_x. Figure 5A (same format as Figs. 2 and 3) illustrates the failure of activation of a sheet with G_x=G_y=20 nS and a size factor of 8 for the central automatic element, which is both below the critical size factor of ≅9 at this value of coupling conductance and below the minimum critical size factor of 8.6 at a coupling conductance of 25 nS (Fig. 4). This simulation is identical to that of Fig. 2B (open diamond labeled “B” in Fig. 4), but is included here for reference. When we now repeat the simulation with G_y lowered to 15 nS (with G_x maintained at 20 nS) we get the successful activation of the sheet shown in Fig. 5B. When, instead of lowering G_y, we increase G_y to 25 nS (again maintaining G_x at 20 nS) we also get successful activation of the sheet, but at a lower rate, as shown in Fig. 5C.

The two results shown in Fig. 5B,C may seem paradoxical, since they show that for an isotropic condition which produced activation failure (G_x=G_y=20 nS, central element size 8) the result is converted into successful activation by either decreasing or increasing G_y. The explanation is that, for a sheet with relatively low values of coupling conductance, we have highly asymmetrical

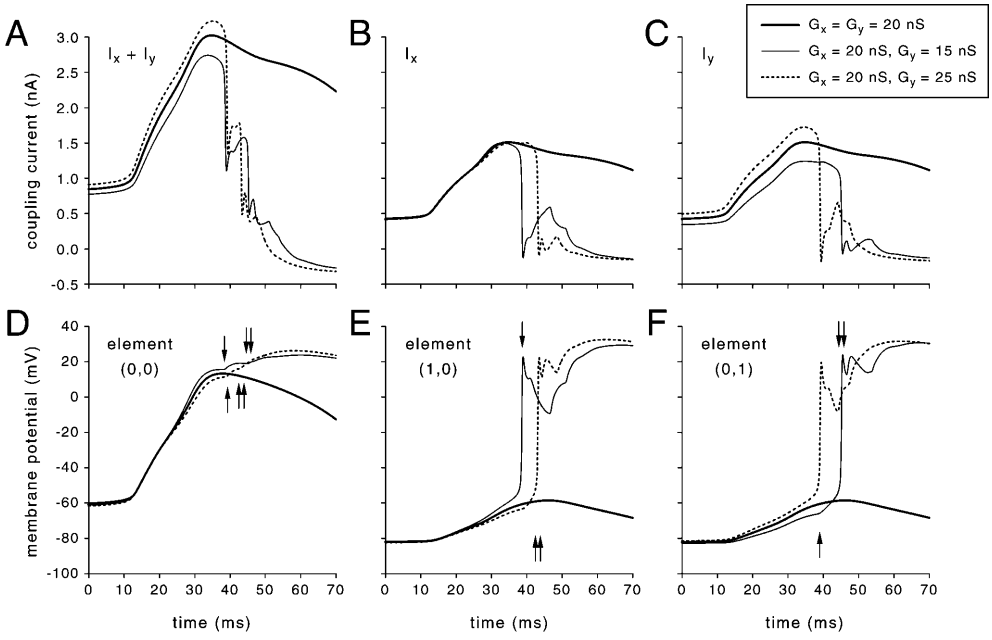

Fig. 6A–F Coupling current (*top panels*) and membrane potential (*bottom panels*) for the central focus element at (0,0) and neighboring elements (1,0) and (0,1) under isotropic conditions (G_x=G_y=20 nS, *thick solid lines*) and upon introduction of anisotropy by either decreasing G_y to 15 nS (*thin solid lines*) or increasing G_y to 25 nS (*dotted lines*). Data shown are for the action potentials of the central focus element indicated with an *asterisk* in Fig. 5. *Single* and *double arrows* indicate points in time. See text for detailed discussion. **A** Total coupling current (I_x+I_y) for element (0,0). **B** Coupling current flowing in the *X* direction (I_x) from element (0,0) to element (1,0). **C** Coupling current flowing in the *Y* direction (I_y) from element (0,0) to element (0,1). **D** Membrane potential of element (0,0). **E** Membrane potential of element (1,0). **F** Membrane potential of element (0,1)

(asynchronous) activation of the sheet that actually decreases the demand for current to activate the entire sheet. This is illustrated in Figs. 6 and 7.

In Fig. 6 we have plotted – for the action potentials of the central focus element indicated with asterisks in Fig. 5 – the total coupling current I_x+I_y for element (0,0) (Fig. 6A) as well as its components flowing in the *X* direction (I_x, Fig. 6B) and *Y* direction (I_y, Fig. 6C). The total coupling current was plotted with a positive value leaving element (0,0), thus producing a repolarization. In Fig. 6D–F, we also included the associated voltage waveforms of elements (0,0), (1,0), and (0,1). To represent the three sets of coupling conductances, we used thick solid lines for the symmetric case (G_x=G_y=20 nS), thin solid lines for the condition in which G_y decreased to 15 nS, and dotted lines for the condition in which G_y increased to 25 nS.

For the symmetric case, neither element (0,1) nor element (1,0) reaches threshold (Fig. 6E, F, thick solid lines). Thus, both adjacent cells continue to act as an electrical load, producing a fast repolarization of the focus element (Fig. 6D, thick solid line), resulting in the short action potential shown in Fig. 5A (asterisk). For each of the asymmetric cases, because both elements (0,1) and (1,0) eventually activate (Fig. 6E and F, thin solid and dotted lines), there are significant changes in the time course of the total coupling current of element (0,0) (Fig. 6A). As either of the adjacent elements (0,1) or (1,0) activates, there is a significant decrease in the outward coupling current from element (0,0), because these adjacent elements are no longer an electrical load, but actually supply current back to element (0,0). Activation of the adjacent elements prevents early repolarization of element (0,0) (Fig. 6D, single- and double-headed arrows) and thus accounts for successful activation of the array for either of the asymmetric conditions. The mechanisms for the activation of these adjacent elements are shown in the middle and right panels of Fig. 6.

In the middle panels of Fig. 6, we plotted the coupling current in the *X* direction for element (0,0) (Fig. 6B) and the membrane potential of element (1,0), which received this current (Fig. 6E). Changing the value of G_y from 20 nS to either 15 or 25 nS did not significantly change the magnitude of the coupling current in the *X* direction before activation of element (1,0) (Fig. 6B). However, the response of the membrane potential of element (1,0) to this current was quite different (Fig. 6E). When G_y was lowered to 15 nS, element (1,0) had a larger voltage response as compared to the symmetric case, which raised the membrane potential to threshold as shown by the thin solid line in Fig. 6E. The larger voltage response of element (1,0) when G_y was lowered was produced by the decreased load on this cell in the *Y* direction through its connections to elements (1,1) and (1,–1), and thus activation of element (1,0) occurred with the decreased G_y value (Fig. 6E, downward single arrow). This activation of element (1,0) then sent current back to element (0,0), preventing early repolarization of element (0,0) (Fig. 6D, downward single arrow). Thus, the activation of element (1,0) led to a greater membrane potential in element (0,0), which then activated, with delay, element (0,1), as

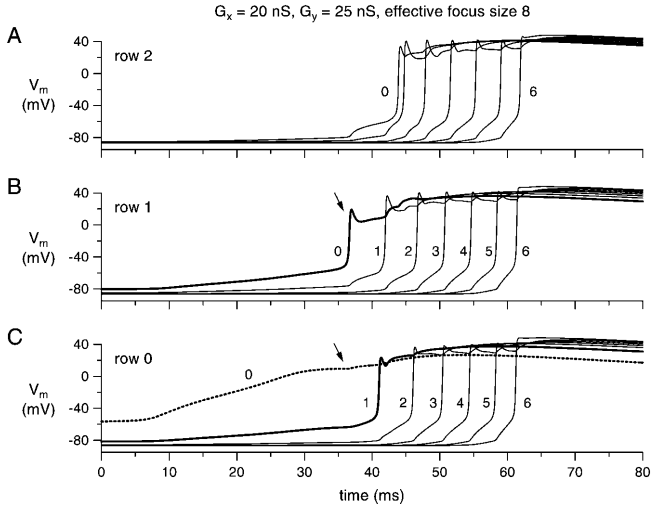

Fig. 7A–C Successful propagation from the central focus element at (0,0) with a size factor of 8 into the two-dimensional sheet of Fig. 1 with G_x=20 nS and G_y=25 nS as shown in Fig. 5C on an expanded time scale. The *three panels* show activation of elements 0, 1, …, 6 (*left* to *right*, labeled "0" through "6") for **A** row 2 (*Y*=2), **B** row 1 (*Y*=1), and **C** row 0 (*middle row*, *Y*=0). *Arrows* in **B** and **C** point to the activation of element (0,1) (*thick solid line* in **B**) which prevents early repolarization of the focus element (0,0) (*dotted line* in **C**) and supports activation of element (1,0) (*thick solid line* in **C**)

shown by the thin solid line in Fig. 6F (downward double arrow).

The right panels of Fig. 6 show the mechanism of successful activation of the array when G_y is increased to 25 nS. Figure 6C shows the coupling current for element (0,0) flowing in the *Y* direction to element (0,1). When G_y is raised or lowered, there is a significant increase or decrease, respectively, of this coupling current. Increases in this coupling current produce a greater response of the membrane potential of element (0,1), as shown by the dotted line in Fig. 6F, and thus lead to activation of element (0,1) (upward single arrow). This activation of element (0,1) then sends current back to element (0,0) and prevents the early repolarization of this element, as shown in Fig. 6D (upward single arrow), which then allows more current to flow in the *X* direction and produces a delayed activation of element (1,0), as shown by the dotted line in Fig. 6E (upward double arrow).

Figure 7 shows the activation pattern for the time period indicated by the horizontal bar in Fig. 5C on an expanded time scale. As in Fig. 5C, Fig. 7C shows the activation of elements 0, 1, …, 6 in the central row ("row 0") of the sheet. The spontaneous activity of the focus element (0,0) appears as a dotted line labeled "0". The activity of the adjacent intrinsically quiescent element (1,0) is plotted as a thick solid line labeled "1". Elements (2,0) through (6,0) activate left to right in time and are plotted as thin solid lines (labeled "2" through "6"). The other two panels of Fig. 7 show the activation of elements 0, 1, …, 6 in rows 1 and 2 of the sheet (Fig. 7B and A, respectively). As indicated by the arrows in Fig. 7B and C, activation of the sheet is asymmetrical, with element (0,1) (thick solid line in Fig. 7B) being activated earlier than element (1,0) (thick solid line in Fig. 7C) as the lower coupling conductance along the *X*-axis inhibits current spread along the *X*-axis and thus delays activation along the *X*-axis. Propagation is more rapid along the *Y*-axis than along the *X*-axis, as illustrated by the earlier activation of element (0,2) (thin line labeled "0" in Fig. 7A) as compared to element (2,0) (thin line labeled "2" in Fig. 7C).

Once activation has succeeded in either direction from the central focus element, the current demand on this focus element is significantly reduced because the element in the direction in which propagation has occurred is no longer a current "sink" but now actually supplies current back to the central element (arrows in Fig. 7B, C). Thus, the presence of anisotropy, by "focusing" current predominantly into one direction of the sheet, shortens the time for which the central element must supply current to the sheet. The elements in the direction that activates first serve to increase the area of cells that have been excited, effectively increasing the size of the focus element as conduction can now proceed from a broader base. This effect is summarized in Figs. 8 and 9.

To delineate the relationship between the values of G_x and G_y and the success or failure of action potential

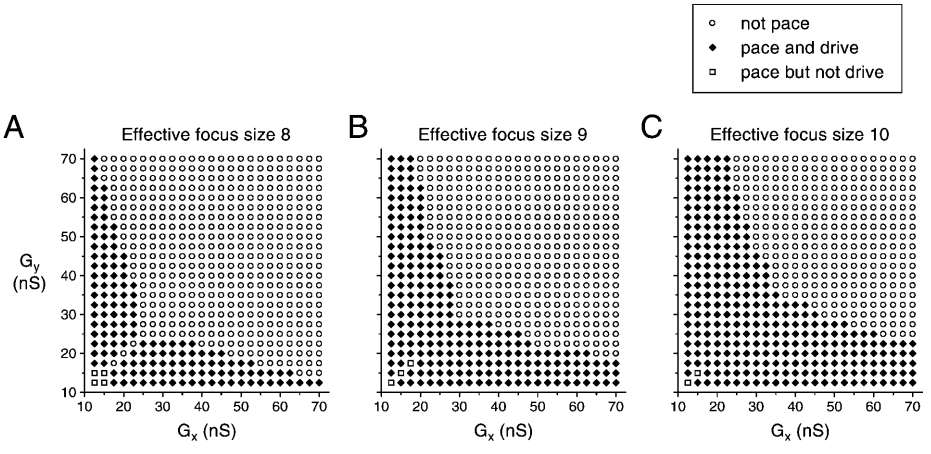

Fig. 8A–C Success or failure of propagation from the central focus element at (0,0) with **A** a size factor of 8, **B** a size factor of 9, or **C** a size factor of 10 into the two-dimensional sheet as diagrammed in Fig. 1 at various combinations of G_x and G_y. Successful propagation ("pace and drive") is indicated with *filled diamonds*. Failure of propagation either occurs as failure to drive ("pace but not drive", *open squares*) or as failure to pace ("not pace", *open circles*)

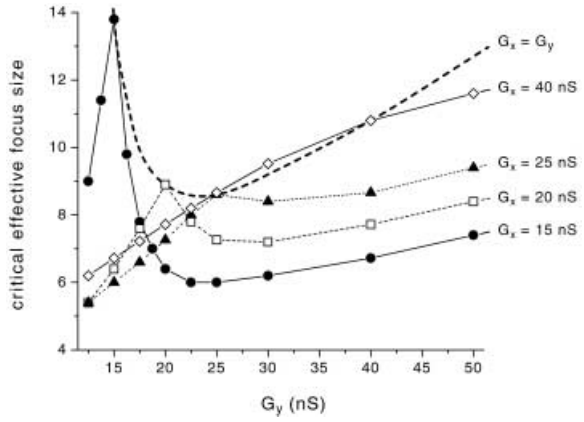

Fig. 9 Critical size factor for successful propagation from the central focus element at (0,0) into the 13×13 element sheet as diagrammed in Fig. 1 with a fixed G_x of 15, 20, 25, or 40 nS as indicated and a variable G_y from 12.5 to 50 nS. The *thick dashed curve* labeled "G_x=G_y" represents the results previously shown in Fig. 4 for the isotropic state

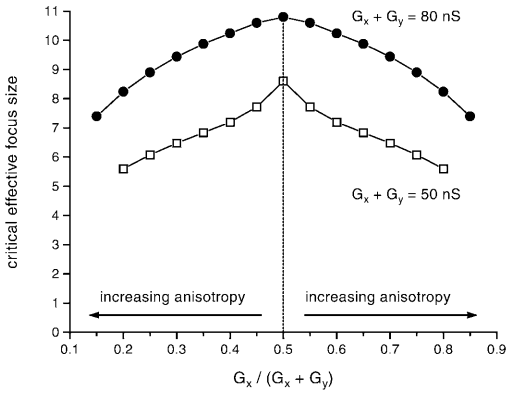

Fig. 10 Critical size factor for successful propagation from the central focus element into the 13×13 element sheet as diagrammed in Fig. 1 as a function of $G_x/(G_x+G_y)$ at total conductance (G_x+G_y) values of 50 and 80 nS (*solid lines with open squares* and *filled circles*, respectively). The *vertical dashed line* indicates the isotropic case of G_x=G_y. The *horizontal arrows* indicate increasing levels of anisotropy

propagation into the sheet, we ran a large number of the simulations illustrated in Fig. 5, maintaining a constant effective focus size. Figure 8 shows results for effective focus sizes of 8, 9, or 10 in panels A, B, and C, respectively. The three possible outcomes "not pace", "pace but not drive", and "pace and drive" are plotted as open circles, open squares, and filled diamonds, respectively. The open symbols along the diagonal in Fig. 8A again show that a focus with effective size 8 fails to propagate into an isotropic sheet at all values of G_x=G_y (see Fig. 4). In an anisotropic sheet with both G_x and G_y≤15 nS (with effective focus size maintained at 8) the limited intercellular current flow inhibits propagation (off-diagonal squares). At relatively high values of G_x (or G_y) >60 nS, propagation is only successful at a high degree of anisotropy (upper left and lower right diamonds). At intermediate values of G_x (or G_y), only moderate degrees of anisotropy are required for successful propagation. At effective focus size 9 (Fig. 8B) or 10 (Fig. 8C), successful propagation can occur in the isotropic case (on-diagonal diamonds), but anisotropy still favors propagation as illustrated by the propagation failing at G_x=G_y=40 nS (total conductance of 80 nS), but being successful at G_x=60 nS and G_y=20 nS (total conductance also 80 nS).

Effects of anisotropy

To delineate the relationship between effective focus size and the degree of anisotropy we fixed G_x at several different values from 15 to 40 nS as shown by the labels in Fig. 9 while we systematically varied G_y and determined the critical size of the focus element that allows activation of the entire sheet. The thick dashed curve labeled "G_x=G_y" is the result previously shown as the solid line with filled squares in Fig. 4 for the isotropic state. For the lowest fixed value of G_x (15 nS, solid line with filled circles) there is a very prominent peak in the relationship, with a maximum in the required critical size of the focus occurring at G_y=15 nS (the isotropic case). For fixed values of G_x of 20 and 25 nS (dashed line with open squares and dotted line with filled triangles, respectively) there is also a maximum in this relationship at the values (G_y=20 and 25 nS, respectively) which make these arrays isotropic. For greater fixed values of G_x (>25 nS, e.g., 40 nS, solid line with open diamonds) there is no such peak at the isotropy value as was seen for the lower values of G_x. Note that for each fixed value of G_x≤ 25 nS there is *facilitation* in the activation of the sheet (requiring a smaller effective focus size) as the value of G_y is made either greater or smaller than the value for isotropy.

The absence of a peak at the isotropy value for fixed values of G_x>25 nS does not imply that the "focusing theory" does not hold for greater fixed values of G_x (and G_y). This is demonstrated in Fig. 10, where we have plotted results of simulations in which both G_x and G_y were varied to induce anisotropy, but in which total conductance in the *X* and *Y* directions (G_x+G_y) was constant. Fig. 10 shows critical focus size as a function of $G_x/(G_x+G_y)$ for G_x+G_y values of 50 and 80 nS (solid lines with open squares and filled circles, respectively). A value of 0.5 for $G_x/(G_x+G_y)$ (dashed vertical line) represents the isotropic case of G_x=G_y. A high degree of anisotropy corresponds with values of $G_x/(G_x+G_y)$ close to 0 (G_x<<G_y; focusing of coupling current in the *Y* direction) or close to 1 (G_x>>G_y; focusing of coupling current in the *X* direction). For total conductance values of either 50 or 80 nS the relationship shows a peak at the $G_x/(G_x+G_y)$ value reflecting isotropy. Note that these peaks correspond with the filled triangle at G_y=25 nS and the open diamond at G_y=40 nS in Fig. 9, respectively. The critical focus size decreases with increasing degree of anisotropy, demonstrating that facilitation in the

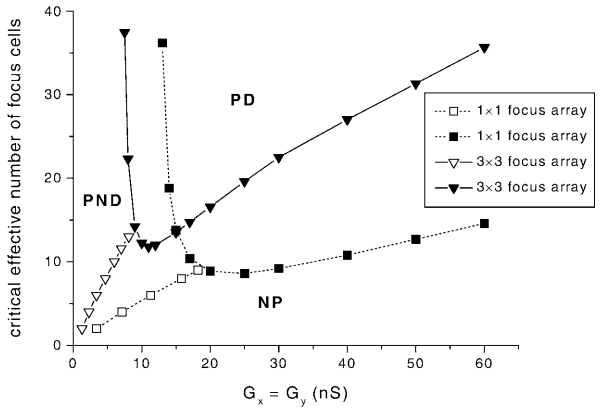

Fig. 11 Effective number of focus cells required for successful propagation into the 13×13 element sheet as diagrammed in Fig. 1 with G_x=G_y, either with a 1×1-element focus (*dotted line with filled squares*) or a 3×3-element focus (*solid line with closed triangles*). Successful propagation occurs for parameter values in the region labeled "*PD*" ("pace and drive"). Failure of propagation either occurs as failure to drive ("pace but not drive", region labeled "*PND*") or as failure to pace ("not pace", region labeled "*NP*"). The *solid line with open triangles* and the *dotted line with open squares* mark the transition between the PND and NP regions for the 3×3-element focus and the 1×1-element focus, respectively

activation of the sheet as the degree of anisotropy is enhanced also occurs at higher values of coupling conductance.

Effects of focus size

In all of the above simulations, we represented the ectopic focus by a single sheet element and modulated its effective size by scaling its coupling currents. This is an idealization we made to simplify the modeling computations. Also, this approach allows our results to be compared with data from experiments in which we incorporated either a real ventricular cell or a real nodal cell as the central element of a two-dimensional sheet of LR model cells [17, 39]. The assumption that the ectopic focus may be represented by a single sheet element composed of a number of infinitely well coupled individual cells affects the simulation results in two ways. First, the magnitude of coupling within the focus region will affect the extent to which the surrounding ventricular cells impose an electrotonic load on the focus. Secondly, and more importantly, the number of direct cell contacts between the focus region and the surrounding cells is not constant, as it is in our simulations, but will increase with increasing focus size, thereby increasing the electrotonic load on the focus.

To test to what extent the assumption of a single element focus had affected our results, we repeated our simulations for Fig. 4 with a 3×3 element focus (filled squares in Fig. 1), directly coupled to 12 ventricular cells instead of 4 (see. Fig. 1), in which the 9 focus elements were of equal effective size and coupled with the same G_x and G_y values as the other elements in the sheet. These data, with focus size again expressed in terms of the effective number of ventricular cells in the focus region, are presented in Fig. 11 as solid lines with open and filled triangles. Figure 11 shows that results are quantitatively, but not qualitatively, different, with the main effect being an underestimation of the critical number of focus cells at higher values of coupling conductance. At lower values of coupling conductance, there is a shift of the relationship to the left. This may be produced by the smaller effective curvature of the wavefront (larger radius of the focus) as the initiation of propagation from the larger central focus encounters the surrounding ventricular cells. However, the conclusion that ectopic focal activity can originate from a region composed of only approximately ten cells still holds.

Discussion

Many studies have examined how structural changes to the myocardium caused by myocardial infarction form a substrate for arrhythmias by forming a structure for reentrant excitation. Such structures include enhanced anisotropy that contributes to the development of spiral waves and wavefront pivoting [8, 12], as well as linear regions of reduced coupling which produce a line of block around which the wavefront can propagate [4, 30]. The main point of the present study is to show how structural changes in the myocardium can affect the initiation of a propagating wave from an ectopic focus.

Scaling of the model

We have used a 49-element sheet to demonstrate the effects of anisotropy on the success or failure of propagation from a central focus element into the sheet. Each element of the sheet is represented by a single cell model, but the size of each element can be scaled such that it represents a number of *N* isopotential cells. With the assumption that each element within the sheet is isopotential, our model is restricted to low degrees of coupling. The values of coupling conductance we used are at least one order of magnitude smaller than the values of gap junctional conductance required for normal conduction in ventricular tissue [14, 31]. Under conditions of myocardial ischemia, discrete groups of surviving cells are separated from other groups of cells by connective tissue [10, 18, 37]. The slow conduction and fractionated waveforms that are characteristic of conduction in ischemic tissue are indications of the successive activation of groups of cells for which the intergroup conductance is limiting the conduction. Our use of a model of elements of variable sizes can be scaled to represent the conduction between groups of cells under the conditions that, within each group, the cells of the group are themselves well coupled to each other and essentially isopotential. That this condition is met under certain ischemic conditions is indicated by the brief duration of each compo-

nent of the fractionated signals and also from direct microelectrode recordings from cells within the groups [18]. Thus, the conduction between groups of 100 cells ("size 100 elements") connected by a conductance of 5 μS would have the same characteristics of electrical loading and also the success or failure of conduction as one would observe between single cells ("size 1 elements") connected by a conductance of 50 nS. In the case of the connections between large groups of cells, the interconnections might be a short bridge of cells, rather than a direct electrical connection between one cell of each group.

Our results show that there is a critical size for the central focus element to produce propagation out into the two-dimensional sheet. For a continuous one- or two-0dimensional system, this would be analogous to the "liminal length" or "liminal area" that must be activated to produce propagation [9, 22, 27, 28]. To further the analogy for discontinuous tissue, the critical size of the central element might be considered the "liminal lump". In terms of the number of collaborating cells within the focus, the minimum size of the focus region for propagation to occur may be as small as approximately ten cells (Fig. 11). This number scales with the number of isopotential cells represented by each element of the sheet. If each element represents 100 cells, the "liminal focus size" would be ≅1000 cells.

It should be emphasized that our model typically holds for conduction between poorly coupled (groups of) cells, as may be observed in peri-infarction zones and remodeled tissue. Our results should not be extrapolated to the case of the continuous conduction that occurs in normal, well-coupled ventricular tissue. In this case, cytoplasmic resistivity and cell geometry play a major role in determining the activation patterns [14, 35]. Simulation of these activation patterns implicates simulation of individual cells by various amounts of cytoplasmic resistors [31, 35].

Activation of an isotropic sheet

We have shown, using a computer model of a thin sheet of myocardium, that propagation from an ectopic focus into an isotropic sheet of ventricular elements requires that the focus be of sufficient size and that there is a biphasic relationship between size of the focus and the coupling conductance throughout the sheet (Fig. 4). When the coupling conductance is small, the ability of the focus to deliver current to the sheet is limited by the amount of coupling between the cells. Thus, the focus must be quite large to provide enough current to bring the neighboring cells to threshold and initiate a propagating wave. As the conductance increases, the critical size of the focus decreases to a minimum value at G_x=G_y=25 nS. At values of conductance larger than 25 nS, the size of the focus increases with increasing conductance. For these larger values of conductance there is an increased electrotonic load on the focus cell inhibiting its ability to spontaneously produce an action potential, thus requiring a larger size for the focus. The minimum critical size factor of the focus model required for successful propagation into an isotropic sheet of LR model cells is 8.6, and this minimum occurs at G_x=G_y=25 nS (Fig. 4). This result is consistent with the results of our recent experimental study [17], in which we demonstrate that a real atrioventricular nodal cell drives an isotropic model atrial sheet more easily than an isotropic model ventricular sheet. In this experimental study, we determined the critical size factor for successful propagation from a real atrioventricular nodal cell in the central location of an isotropic 7×7 sheet of LR model cells, and found that this critical size factor (also corrected for differences in cell size between nodal and ventricular cells; see "Materials and methods") was 7.4±2.0 (mean ±SEM, n=8) and occurred at G_x=G_y=20 nS.

The results summarized in Fig. 4 demonstrate that successful initiation of a propagating wave occurs only for intermediate values of coupling conductance. In their study of ectopic beating resulting from a centrally positioned region of sodium-overloaded cells in a two-dimensional sheet of atrial cells Winslow et al. [43] also observed a "window" of coupling conductance values allowing propagation of the ectopic beats (their Fig. 4). In a recent modeling study, Saiz et al. [29] obtained similar results. They modeled a strand of cardiac cells using the LR model where half the strand was set to be able to produce early afterdepolarizations (EADs) while the other half was set to control conditions. The coupling conductance between the two halves of the strand was varied and propagation of EADs as ectopic beats occurred only for intermediate values of conductance. At small values of conductance the EADs were unable to propagate and at large values of conductance the EADs were suppressed.

Activation of an anisotropic sheet

In a recent experimental study [39] we determined the critical size factor for successful propagation from a *directly stimulated* (not spontaneously active) real ventricular cell in the central location of a 7×7 sheet of LR model cells, and found that this critical size factor was ≅7 in the isotropic case of G_x=G_y=30 nS and decreased when anisotropy was present compared to the isotropic case. These results are consistent with the results of our present study, in which this size factor was ≅9 for a spontaneously active cell model as the central element of the sheet (Fig. 4). Our results are also consistent with our earlier study where we coupled our SAN model [40] to an isolated rabbit ventricular cell [38]. We showed that the SAN model had to be of sufficient size and that coupling conductance needed to be of an intermediate value for propagation of the focus to occur. The present study has theoretically extended that work, and shows that the two-dimensional geometry of a sheet of cells can alter the ability of an ectopic focus to propagate.

Altering the geometry of the sheet to include anisotropy enhances the ability of the ectopic focus to initiate a propagating wave by allowing a "focusing" of the coupling current which is then able to bring the neighboring cells to threshold. Introducing anisotropy into the sheet by either decreasing or increasing conductance in one direction causes an asynchrony in the propagation; thus, activation of a cell in the direction of the higher conductance decreases the load on the focus cell (because the cell in that direction has activated) and helps to provide current for activation of the rest of the sheet. This facilitation of propagation upon introduction of anisotropy by either decreasing or increasing G_y while maintaining a constant value of G_x is only observed at G_x values ≤25 nS (Fig. 9). At higher values of coupling conductance direct loading effects predominate and an increase in G_y leads to an increase in the critical focus size required for successful propagation. However, the "focusing theory" still holds, as shown in Fig. 10: under conditions of constant load (constant G_x+G_y), critical focus size is maximal in the isotropic case and decreases with increasing anisotropy.

Both resistive barriers and enhanced anisotropy are results of myocardial infarction [4, 30]. Aging can also increase the degree of anisotropy as was shown by Spach and Dolber [33]. They showed, in human atrial pectinate muscle, that increasing age increases the longitudinal versus transverse conduction velocity ratio and that this increase correlates with a greater amount of collagenous septa separating the muscle into small fiber bundles in the older muscle. Our simulation results suggest that this underlying structure caused by infarction or aging may facilitate the development of ectopic activity when the membrane properties of some portion of the myocardium are altered in such a way as to become spontaneously active in subsequent ischemic events. This arrhythmogenic effect may be counteracted by a reduction in anisotropy due to rearrangement of gap junctions in response to ischemia [10, 32].

Limitations

The present modeling study has several limitations. First, we chose the LR ventricular cell model as a specific ventricular cell model and the SAN model to create a specific ectopic focus model. The quantitative results of our simulations are of course dependent on the membrane models chosen. However, the conclusion that anisotropy may reduce the electrotonic load on the ectopic focus and thus facilitate propagation from an ectopic focus into a sheet of myocardium should not depend on the membrane models chosen, and should hold for any region of focal activity. Secondly, we chose to modulate effective focus size by scaling coupling currents, thus neglecting the effects of the increase in number of cell contacts with an increase in focus size. This approach allows direct comparison with our previous experimental data [17, 39], but it also affects the quantitative results of our simulations (see Fig. 11). Additionally, the requirement of symmetry to decrease the number of elements required for the simulation limits the distribution of conductances. Although it would be interesting to include heterogeneous distribution of coupling conductances into the sheet model, the current implementation is sufficient to show how the presence of anisotropy can enable an ectopic focus to initiate a propagating wave into a sheet.

Finally, our simulations are based on the assumption that a single cell is, for these low values of coupling conductance, very nearly isopotential, as demonstrated by the theoretical work of Shaw and Rudy [31]. Therefore each "element" is an intact cell and the actual spatial dimensions and orientation of the particular cells used do not affect the results. We have deliberately chosen lower values of coupling conductance than those occurring in "normal" ventricular tissue in order to emphasize the effects which might be observed in cells that are partly uncoupled, such as might have occurred by prior ischemia. Also, these low values of coupling conductance, and the resulting discontinuous conduction, allowed us to use relatively small arrays to demonstrate these effects.

Acknowledgements This work was partially supported by the Research Council for Earth and Life Sciences (ALW) with financial aid from the Netherlands Organization for Scientific Research (NWO), NIH grant HL22562, an American Heart Association Fellowship, and the Emory Egleston Children's Research Center.

References

1. Cai D, Winslow RL, Noble D (1994) Effects of gap junction conductance on dynamics of sinoatrial node cells: two-cell and large-scale network models. IEEE Trans Biomed Eng 41:217–231
2. Clerc L (1976) Directional differences of impulse spread in trabecular muscle from mammalian heart. J Physiol (Lond) 255:335–346
3. de Bakker JM, Hauer RN, Bakker PF, Becker AE, Janse MJ, Robles de Medina EO (1994) Abnormal automaticity as mechanism of atrial tachycardia in the human heart – electrophysiologic and histologic correlation: a case report. J Cardiovasc Electrophysiol 5:335–344
4. Dillon SM, Allessie MA, Ursell PC, Wit AL (1988) Influences of anisotropic tissue structure on reentrant circuits in the epicardial border zone of subacute canine infarcts. Circ Res 63:182–206
5. Fast VG, Kléber AG (1994) Anisotropic conduction in monolayers of neonatal rat heart cells cultured on collagen substrate. Circ Res 75:591–595
6. Fast VG, Kléber AG (1995) Cardiac tissue geometry as a determinant of unidirectional conduction block: assessment of microscopic excitation spread by optical mapping in patterned cell cultures and in a computer model. Cardiovasc Res 29: 697–707
7. Fast VG, Kléber AG (1995) Block of impulse propagation at an abrupt tissue expansion: evaluation of the critical strand diameter in 2- and 3-dimensional computer models. Cardiovasc Res 30:449–459
8. Fast VG, Kléber AG (1997) Role of wavefront curvature in propagation of cardiac impulse. Cardiovasc Res 33:258–271
9. Fozzard HA, Schoenberg M (1972) Strength-duration curves in cardiac Purkinje fibres: effects of liminal length and charge distribution. J Physiol (Lond) 226:593–618

10. Gardner PI, Ursell PC, Fenoglio JJ, Wit AL (1985) Electrophysiologic and anatomic basis for fractionated electrograms recorded from healed myocardial infarcts. Circulation 72: 596–611
11. Goodman D, Steen AB, Dam RT (1971) Endocardial and epicardial activation pathways of the canine right atrium. Am J Physiol 220:1–11
12. Gray RA, Jalife J, Panfilov A, Baxter WT, Cabo C, Davidenko JM, Pertsov AM (1995) Nonstationary vortexlike reentrant activity as a mechanism of polymorphic ventricular tachycardia in the isolated rabbit heart. Circulation 91:2454–2469
13. Hoyt RH, Cohen ML, Saffitz JE (1989) Distribution and three-dimensional structure of intercellular junctions in canine myocardium. Circ Res 64:563–574
14. Jongsma HJ, Wilders R (2000) Gap junctions in cardiovascular disease. Circ Res 86:1193–1197
15. Joyner RW, Ramon F, Morre JW (1975) Simulation of action potential propagation in an inhomogeneous sheet of coupled excitable cells. Circ Res 36:654–661
16. Joyner RW, van Capelle FJL (1986) Propagation through electrically coupled cells. How a small SA node drives a large atrium. Biophys J 50:1157–1164
17. Joyner RW, Wang Y-G, Wilders R, Golod DA, Wagner MB, Kumar R, Goolsby WN (2000) A spontaneously active focus drives a model atrial sheet more easily than a model ventricular sheet. Am J Physiol 279:H752–H763
18. Kienzle MG, Tan RC, Ramza BM, Young ML, Joyner RW (1987) Alterations in endocardial activation of the canine papillary muscle early and late after myocardial infarction. Circulation 76:860–874
19. Kléber AG, Janse MJ, Wilms-Schopmann FJG, Wilde AAM, Coronel R (1986) Changes in conduction velocity during acute ischemia in ventricular myocardium of the isolated porcine heart. Circulation 73:189–198
20. Kumar R, Wilders R, Joyner RW, Jongsma HJ, Verheijck EE, Golod DA, van Ginneken ACG, Goolsby WN (1996) An experimental model for an ectopic focus coupled to ventricular cells. Circulation 94:833–841
21. Leon LJ, Roberge FA, Vinet A (1994) Simulation of two-dimensional anisotropic cardiac reentry effects of the wavelength on the reentry characteristics. Ann Biomed Eng 22: 592–609
22. Lindemans FW, Denier van der Gon JJ (1978) Current thresholds and liminal size in excitation of heart muscle. Cardiovasc Res 12:477–485
23. Luke RA, Beyer EC, Hoyt RH, Saffitz JE (1989) Quantitative analysis of intercellular connections by immunohistochemistry of the cardiac gap junction protein connexin43. Circ Res 65:1450–1457
24. Luke RA, Saffitz JE (1991) Remodeling of ventricular conduction pathways in healed canine infarct border zones. J Clin Invest 87:1594–1602
25. Luo CH, Rudy Y (1994) A dynamic model of the cardiac ventricular action potential. I. Simulations of ionic currents and concentration changes. Circ Res 74:1071–1096
26. Myerburg RJ, Kessler KM, Castellanos A (1994) Interactions between structure and function in sudden cardiac death. In: Akhtar M, Myerburg RJ, Ruskin JN (eds) Sudden cardiac death. Williams and Wilkins, Philadelphia, pp 32–47
27. Noble D (1972) The relation of Rushton's "liminal length" for excitation to the resting and active conductances of excitable cells. J Physiol (Lond) 226:573–591
28. Pressler ML (1984) Cable analysis in quiescent and active sheep Purkinje fibres. J Physiol (Lond) 352:739–757
29. Saiz J, Ferrero JMJ, Monserrat M, Ferrero JM, Thakor NV (1999) Influence of electrical coupling on early afterdepolarizations in ventricular myocytes. IEEE Trans Biomed Eng 46:138–147
30. Schalij MJ, Lammers WJ, Rensma PL, Allessie MA (1992) Anisotropic conduction and reentry in perfused epicardium of rabbit left ventricle. Am J Physiol 263:H1466–H1478
31. Shaw RM, Rudy Y (1997) Ionic mechanisms of propagation in cardiac tissue. Roles of the sodium and L-type calcium currents during reduced excitability and decreased gap junction coupling. Circ Res 81:727–741
32. Smith JH, Green CR, Peters NS, Rothery S, Severs NJ (1991) Altered patterns of gap junction distribution in ischemic heart disease. An immunohistochemical study of human myocardium using laser scanning confocal microscopy. Am J Pathol 139:801–821
33. Spach MS, Dolber PC (1985) The relation between discontinuous propagation in anisotropic cardiac muscle and the "vulnerable period" of reentry. In: Zipes DP, Jalife J (eds) Cardiac electrophysiology and arrhythmias. Harcourt Brace Jovanovich, New York, pp 241–252
34. Spach MS, Heidlage JF (1995) The stochastic nature of cardiac propagation at a microscopic level. Electrical description of myocardial architecture and its application to conduction. Circ Res 76:366–380
35. Spach MS, Heidlage JF, Dolber PC, Barr RC (2000) Electrophysiological effects of remodeling cardiac gap junctions and cell size: experimental and model studies of normal cardiac growth. Circ Res 86:302–311
36. Spach MS, Miller WT, Miller-Jones E, Warren RB, Barr RC (1979) Extracellular potentials related to intracellular action potentials during impulse conduction in anisotropic canine cardiac muscle. Circ Res 45:188–204
37. Ursell PC, Gardner PI, Albala A, Fenoglio JJ, Wit AL (1985) Structural and electrophysiological changes in the epicardial border zone of canine myocardial infarcts during infarct healing. Circ Res 56:436–451
38. Wagner MB, Golod D, Wilders R, Verheijck EE, Joyner RW, Kumar R, Jongsma HJ, van Ginneken ACG, Goolsby WN (1997) Modulation of propagation from an ectopic focus by electrical load and by extracellular potassium. Am J Physiol 272:H1759–H1769
39. Wang Y-G, Kumar R, Wagner MB, Wilders R, Golod DA, Goolsby WN, Joyner RW (2000) Electrical interactions between a real ventricular cell and an anisotropic two-dimensional sheet of model cells. Am J Physiol 278:H452–H460
40. Wilders R, Jongsma HJ, van Ginneken ACG (1991) Pacemaker activity of the rabbit sinoatrial node. A comparison of mathematical models. Biophys J 60:1202–1216
41. Wilders R, Kumar R, Joyner RW, Jongsma HJ, Verheijck EE, Golod DA, van Ginneken ACG, Goolsby WN (1996) Action potential conduction between a ventricular cell model and an isolated ventricular cell. Biophys J 70:281–295
42. Wilders R, Verheijck EE, Kumar R, Goolsby WN, van Ginneken ACG, Joyner RW, Jongsma HJ (1996) Model clamp and its application to synchronization of rabbit sinoatrial node cells. Am J Physiol 271:H2168–H2182
43. Winslow RL, Varghese A, Noble D, Adlakha C, Hoythya A (1993) Generation and propagation of ectopic beats induced by spatially localized Na-K pump inhibition in atrial network models. Proc R Soc Lond B Biol Sci 254:55–61
44. Zeng J, Laurita KR, Rosenbaum DS, Rudy Y (1995) Two components of the delayed rectifier K^+ current in ventricular myocytes of the guinea pig type. Theoretical formulation and their role in repolarization. Circ Res 77:140–152